ELSEVIER

Carbohydrate Research 273 (1995) 157–170

CARBOHYDRATE RESEARCH

Determination by NMR spectroscopy of the structure and conformational features of the enterobacterial common antigen isolated from *Escherichia coli*

Marta Bruix [a,*], Jesús Jiménez-Barbero [b], Philippe Cronet [c]

[a] *Instituto de Estructura de la Materia, C.S.I.C., Madrid, Spain*
[b] *Instituto de Química Orgánica, C.S.I.C., Madrid, Spain*
[c] *European Molecular Biology Laboratory, Heidelberg, Germany*

Received 14 November 1994; accepted 2 February 1995

Abstract

Complete ^{1}H and ^{13}C spectrum of a polysaccharide isolated from *Escherichia coli*, which is the major component of the enterobacterial common antigen, has been analyzed through two-dimensional nuclear magnetic resonance spectroscopy. In addition, distance constraints from NOESY and ROESY experiments have been combined with molecular dynamic simulations to determine its major conformation in water solution. Data resulting from both free dynamic simulations and restrained dynamic simulations have been compared with experimental data and discussed.

Keywords: Sugar conformation; Enterobacterial common antigen (ECA); ECA structure; NMR of ECA

1. Introduction

The enterobacterial common antigen (ECA) is a polysaccharide antigen elaborated by most wild-type strains of Enterobacteriaceae [1]. This polysaccharide is present in the surface of these bacteria where it is acting as a hapten. It is therefore of crucial

* Corresponding author.

SSDI 0008-6215(95)00117-4

importance for the molecular recognition of some pathogenic bacteria by the host and, in addition, it has been demonstrated to be the basis of the detection of enterobacterial contamination in water [2].

The trisaccharide-repeating unit of the major component of this antigen was identified some years ago [3] by analytical characterization of partially hydrolized derivatives isolated from *Shigella sonnei* phase I. There has been some controversy on the structure of ECAs isolated from different sources. Thus, two different forms of ECA, a linear [4] and a cyclic polysaccharide [5,6], have been subsequently reported and their chemical composition and sequence have been studied by nuclear magnetic resonance (NMR) and mass spectrometry methods.

Although the assignment of the proton and carbon NMR spectra of different ECAs have been reported within those studies no attempts for the determination of its three-dimensional structure by NMR methods have been published. Current opinion in oligosaccharide conformational analysis indicates that there is certain flexibility around the glycosidic bonds of linear oligosaccharides [7]. Therefore, the NMR parameters correspond to an average of the different conformations existing in solution. Different approaches exist nowadays to carry out three dimensional studies of oligo- and poly-saccharides. Some authors have compared experimental NMR data with the NMR parameters derived from statistical–mechanical analysis of molecular mechanics and dynamics calculations [8]. On the other hand, it has been also proposed the use of molecular dynamics simulations which include distance restraints, obtained from experiments, to study the conformational behavior of carbohydrates [9]. Both approaches try to circumvent the frequent problem of obtaining virtual conformations [10], that is, a structure which satisfies the experimental data, but which may not have physical significance. In addition, there is much controversy on the validity and scope of the force fields currently used for carbohydrate conformational analysis [11], which implies the lack of total confidence in the results provided by the calculations, when no experimental data are available.

The present work was undertaken to obtain information about the solution structure of the ECA polysaccharide. Thus, on the basis of the complete NMR assignment and the accurate evaluation of nuclear Overhauser effects (NOEs), we now report the study of its conformational features by using NMR spectroscopy assisted by restrained and unrestrained molecular dynamic (MD) simulations.

2. Results and discussion

NMR assignment and sequence.—The ^{1}H NMR spectrum of **1** showed three strong signals corresponding to anomeric protons indicating that the polysaccharide has a trisaccharide-repeating unit. The signals appear at 4.86 ppm (unit A), 4.97 ppm (unit B) and 5.12 ppm (unit C). The majority of the signals in the ^{1}H NMR spectrum were easily assigned through correlation spectroscopy (COSY) and total correlation spectroscopy (TOCSY) techniques, starting from the anomeric proton resonances (Fig. 1). One aliphatic methyl resonance was evident as a doublet at 1.05 ppm, (unit C) while two

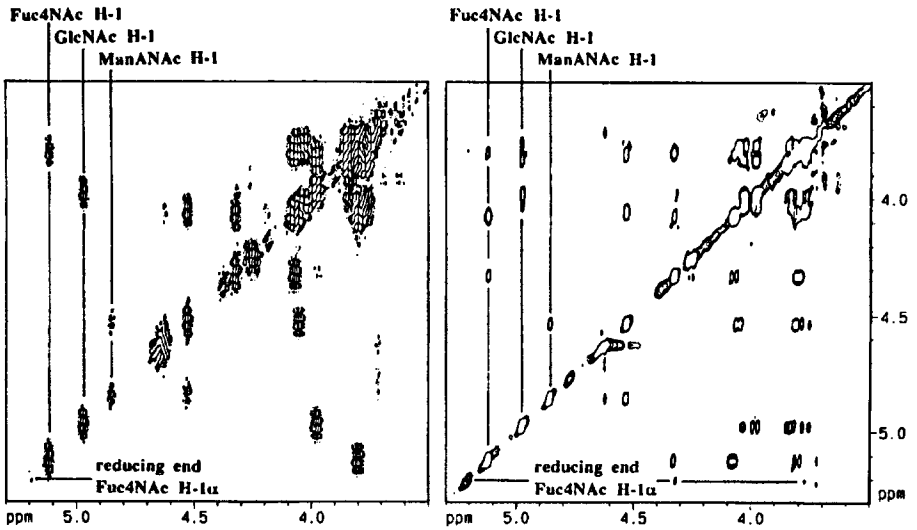

Fig. 1. Sections of a COSY (left) and TOCSY (right) spectra of compound **1** in D_2O at 25°C and pH 7.0. Direct and relayed scalar connectivities for H-1 protons are indicated.

singles were present at 2.02 and 2.08 ppm (double intensity), indicating the presence of three acetyl methyl groups. These signals belong in fact to acetamido groups, since the COSY spectrum obtained in H_2O showed the presence of three HN resonances at 7.86, 7.93 and 8.32 ppm respectively. The combination of TOCSY, COSY, and the heteronuclear single and multiple-quantum coherence (HSMQC) technique, showed that two acetamido groups are joined to position 2 of A and B pyranoid rings, while the remaining one is attached to position 4 of ring C. Only one hydroxymethyl group is present, that of moiety B, and thus position 6 of unit A is oxidized in form of a carboxyl group. As stated above, position 6 of unit C is a methyl group.

The estimation of the vicinal proton–proton coupling constants for the different rings from the cross-peaks patterns (active and passive couplings) in combination with the intraresidue NOE contacts showed the presence of a 2-acetamido-2-deoxy-β-D-mannuronic acid moiety (unit A), a 2-acetamido-2-deoxy-α-D-glucosyl residue (unit B) and a 4-acetamido-4,6-dideoxy-α-D-galactosyl residue (unit C). The analysis of the carbon chemical shifts indicated unequivocally that unit A and B are substituted at position 4, while fragment C is substituted at position 3.

Finally, the study of the NOE contacts from the anomeric protons (Fig. 2) showed spatial proximity between H-1 of ring A with H-4 and H-6 of unit B, H-1 of unit B and H-3 and H-4 of unit C, and H-1 of unit C and H-4 of unit A. Therefore, it can be safely concluded that the repeating unit of the polysaccharide is –A–B–C–. The NOE pattern is completely consistent with the substitution estimated from the HSMQC experiment (^{13}C chemical shifts) and is also in agreement with the presence of D-sugars.

Proton NMR spectra also contained weaker signals for terminal sugar residues (Fig. 1). The terminal α-reducting end was identified as a unit C-like with anomeric protons at 5.23 ppm (α anomer) and 4.77 ppm (β anomer). A careful integration of anomeric

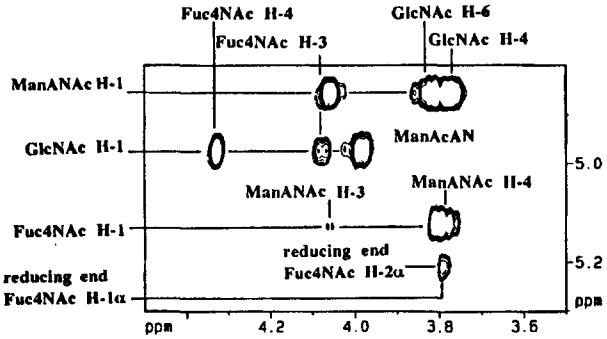

Fig. 2. Portion of the NOESY spectrum (150 ms) of compound **1** in D_2O at 25°C and pH 7.0. NOE inter-residue connectivities from the anomeric protons are labeled.

signals gave a ratio compatible with a linear sequence **1** with the unit A–B–C repeated four times:

$$[\rightarrow 4)\text{-}\beta\text{-ManA}p\text{NAc}(1\rightarrow 4)\text{-}\alpha\text{-D-Glc}p\text{NAc}\text{-}(1\rightarrow 3)\text{-}\alpha\text{-D-Fuc}p4\text{NAc}\text{-}(1\rightarrow]_4$$
$$\text{A} \qquad\qquad \text{B} \qquad\qquad \text{C}$$

1

This glycosidic sequence allowed us to identify the linear polysaccharide **1** as the major component of the enterobacterial common antigen. The assignments carried out in this work are shown in Table 1 and are in general accordance with those previously reported for ECA [4–6].

Conformational analysis.—NOESY and ROESY experiments were conducted for the polysaccharide at 25°C. The NOESY cross peaks were negative, that is, they showed the same sign as the diagonal peaks. Thus, the global correlation time is in the nanoseconds

Table 1
^1H and ^{13}C NMR chemical shifts (δ, ppm) for **1** in D_2O at 25°C and pH 7.0

Atom	Sugar			
	ManANAc	GlcNAc	Fuc4NAc	Fuc4NAc (α reducing end)
H-1	4.86	4.97	5.12	5.23
H-2	4.53	3.98	3.80	3.79
H-3	4.06	3.84	4.07	4.00
H-4	3.77	3.78	4.33	4.31–4.33
H-5	3.82	4.03	4.26	4.31–4.33
H-6	—	3.86,3.78	1.05	1.06
C-1	100.6	95.0	102.9	
C-2	54.9	55.0	69.3	
C-3	73.8	71.1	73.8	
C-4	79.9	80.1	51.6	
C-5	79.3	72.2	68.1	
C-6	178.0	61.7	17.0	

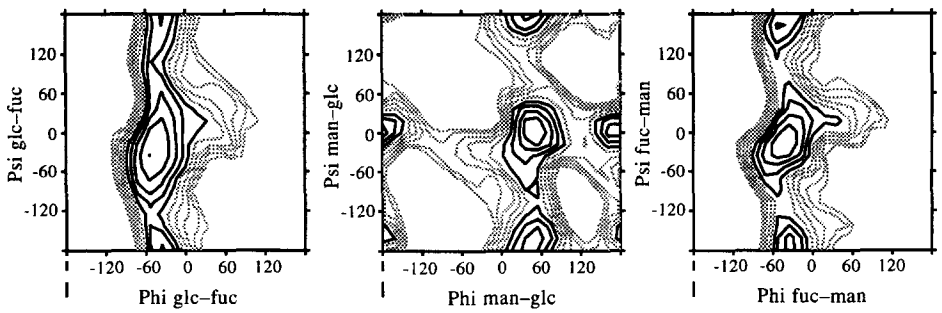

Fig. 3. Relaxed-residue potential energy surfaces of the disaccharide model fragments of compound **1**. Left: GLc*p*NAc-α-(1 → 3)-Fuc*p*4NAc. Centre: ManA*p*NAc-β-(1 → 4)-GlcpNAc. Right: Fuc*p*4NAc-α-(1 → 4)-ManA*p*NAc.

time scale, as expected for a high molecular weight sample [12]. Intra- and inter-residue enhancements were quantified from the rows corresponding to the anomeric protons and the other well resolved protons in the 2D-NMR spectra. Signal overlap was not a major problem in accurate quantification and inter-residue proton–proton distances were estimated by using the isolated spin pair approximation which, for the mixing time used in the NOESY experiment (150 ms), seems to be accepted [12]. The ROESY experiment was interpreted only in a qualitative way, since several spurious Hartmann–Hahn transfers were evident which precluded a quantitative analysis of the enhancement. It is well known that Hartmann–Hahn transfer is a major problem when analyzing ROESY spectra of oligosaccharides [13].

The first step in the conformational study was to generate potential energy surfaces for every linkage of the polysaccharide, i.e. ManA*p*NAc-(1 → 4)-Glc*p*NAc (ManANAc-GlcNAc), Glc*p*NAc-(1 → 3)-Fuc*p*4NAc (GlcNAc-Fuc4NAc) and Fuc*p*4NAc-(1 → 4)-ManA*p*NAc (Fuc4NAc-ManANAc). Relaxed residue energy plots of the isoenergy contours, using the AMBER programme as modified for carbohydrates [14], are given in Fig. 3. It can be observed that the maps for ManANAc-GlcNAc and Fuc4NAc-ManANAc are those which occupy a larger area, while that of GlcNAc-Fuc4NAc is more restricted. The lowest energy region (below 5 Kcal/mol from the global minimum) of ManANAc-GlcNAc is described by $\Phi = 60 \pm 60°$, $\Psi = 0 \pm 35°$, and $r_{\text{H-1-H-4}} = 2.4 \pm 0.4$ Å, typical of equatorial $\beta(1 \rightarrow 4)$ linkages [15], appears to be populated in more than 90% extent, while there is a small island centered about Φ, $\Psi = 50, -170°$, which is populated less than 5% at 40°. For Fuc4NAc-ManANAc, the low energy region is described by torsion angles $\Phi = -10 \pm 70°$, $\Psi = 0 \pm 60°$, and is populated in more than 95% extent. The rest of the population derives from this region towards an island at Φ, $\Psi = -60,180°$. Finally, two regions are populated for GlcNAc-Fuc4NAc. One is centered around $\Phi = 25 \pm 40°$, $\Psi = 20 \pm 30°$, while the other one has $\Phi = -50 \pm 10°$, $\Psi = -50 \pm 20°$. It has to be noted that all these populations are calculated from steric energy values which correspond to enthalpies and not to true free energies.

As a further step, one heptasaccharide fragment of **1**, ManANAc-GlcNAc-Fuc4NAc-ManANAc-GlcNAc-Fuc4NAc-ManANAc, was built from the global minima of the

Table 2
Calculated (from MD simulations) and experimental (from NOESY experiments) distances for the relevant interresidue proton pairs of compound **1** in D_2O

Proton Pair	Distance			
	MD (restrained)	MD (unrestrained)	I.S.P.A.	Restriction
Fuc4NAc-H-3/GlcNAc-H-1	2.67 [a], 2.60 [b]	2.73 [a], 2.80 [b]	2.65	2.3–3.1
Fuc4NAc-H-4/GlcNAc-H-1	2.61, 2.42	3.12, 2.38	2.45	2.0–2.7
ManANAc-H-4/Fuc4NAc-H-1	2.35, 2.61	2.30, 2.71	2.40	2.0–2.7
ManANAc-H-3/Fuc4NAc-H-1	3.70, 2.98	3.31, 3.41	3.35	3.0–3.7
GlcNAc-H-4/ManANAc-H-1	2.42, 2.35	2.43, 3.39	2.40	2.0–2.7
GlcNAc-H-3/ManANAc-H-1	3.50, 3.31	3.23, 2.25		
GlcNAc-H-6_a/ManANAc-H-1	4.03, 2.89	4.06, 4.24	2.90	
GlcNAc-H-6_b/ManANAc-H-1	3.62, 2.87	4.36, 4.32		

[a] The first value refers to the first disaccharide moiety of the heptasaccharide model.
[b] The second value refers to the second disaccharide moiety ofthe heptasaccharide model.

different maps and after extensive minimization, its conformational stability was studied by using molecular dynamics simulations with the DISCOVER-AMBER program [16].

Restrained trajectory.—First, a MD simulation was performed with weak NOE-derived interproton constraints as displayed in Table 2. The trajectories of the different glycosidic linkages are displayed in Fig. 4. In all cases, no chair-to-chair or chair-to-boat interconversions were observed. Starting from the non-reducing end, the average Φ/Ψ angles (Table 3) were ManANAc-GlcNAc, $50/-30$, GlcNAc-Fuc4NAc, $-90/-20$, Fuc4NAc-ManANAc, $-36/-17$, ManANAc-GlcNAc, $55/-10$, GlcNAc-Fuc4NAc, $-60/-40$, Fuc4NAc-ManANAc, $30/-20$. Therefore, there are not major differences in the conformational behavior of the analogous linkages although some distinct characteristics are appreciable. For both ManANAc-GlcNAc, it can be observed that the trajectories remained most of the time in the broad low energy region previously mentioned, with Φ values in agreement with the exo-anomeric effect, although for the terminal non-reducing linkage important excursions to somehow negative Ψ angles are observable. The transitions observed for the GlcNAc-Fuc4NAc fragments are quite similar, Φ angle is fairly constant around the exo-anomeric value, while Ψ oscillates between 0 and moderately negative values, always within the low energy region. Finally, while the internal Fuc4NAc-ManANAc moiety presents a rather constant trajectory around $\Phi/\Psi = -40/-15$ after the equilibration period, the terminal one shows several transitions between the two major minima included within the low energy region.

The corresponding average distances obtained for the simulation from $\langle r^{-6} \rangle$ values are shown in Table 2. It can be observed that the distances for the ManANAc-GlcNAc fragment shows fair agreement between the experimental and theoretical interproton

Fig. 4. Molecular dynamics Φ/Ψ trajectories corresponding to the restrained simulation of the heptasaccharide model. Panels refer to the following linkages: MG, Man*A*p*N*Ac-(1 → 4)-Glc*p*NAc; GF, Glc*p*NAc-(1 → 3)-Fuc*p*4NAc and FM, Fuc*p*4NAc-(1 → 4)-Man*A*p*N*Ac. Starting from the non-reducting end, the first linkage of each type is numbered as 1 and the second as 2.

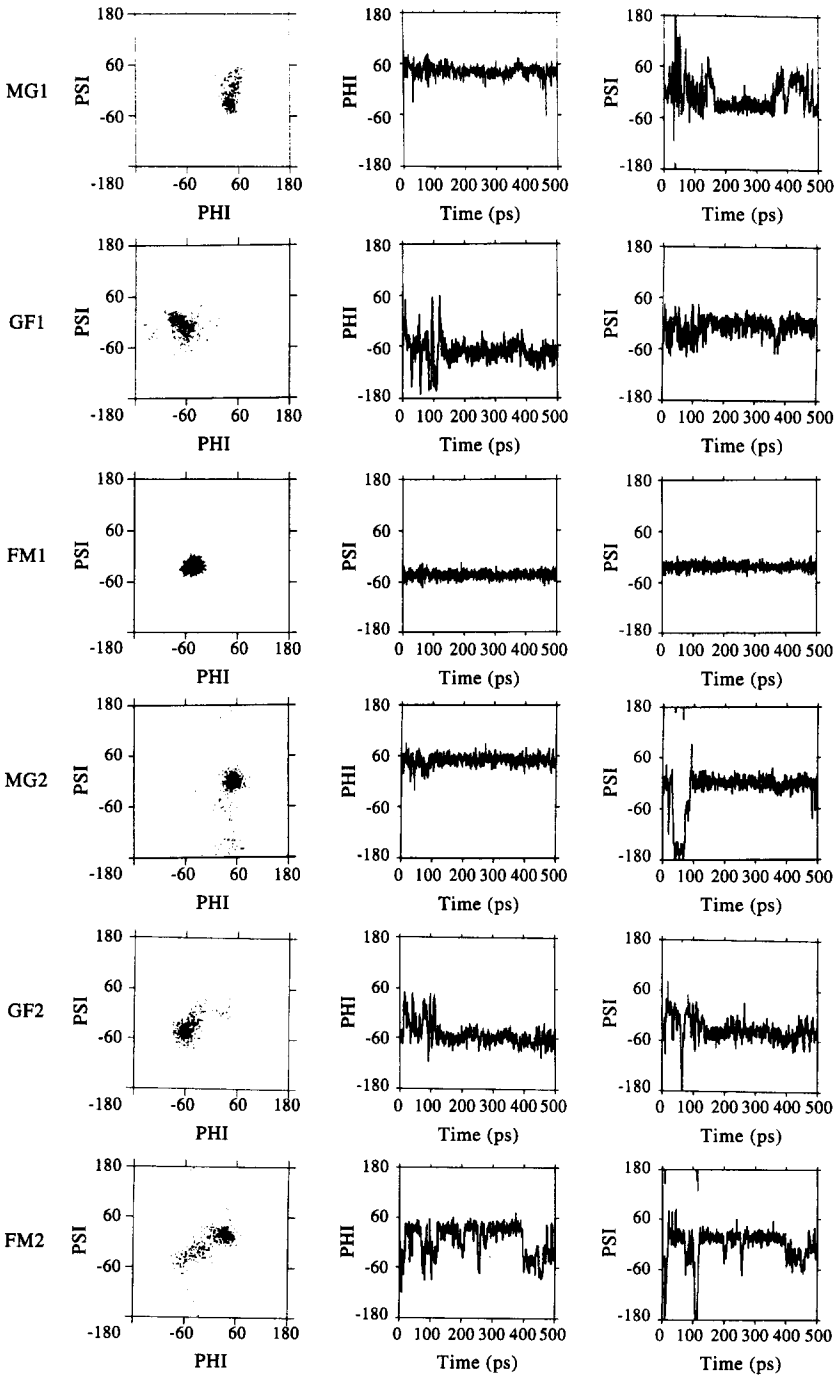
MG1
GF1
FM1
MG2
GF2
FM2
PSI
PHI
Time (ps)
180
60
-60
-180
0 100 200 300 400 500

Table 3
Average Φ/Ψ angles (°) during the restrained and unrestrained MD simulations of the heptasaccharide model of compound **1**

Fragment	Φ/Ψ (°)		
	Starting	Restrained	Unrestrained
ManANAc-GlcNAc	54/1 [a], −37/−24 [b]	50/−30, 55/−10	55/−15, 55/−150
GlcNAc-Fuc4NAc	−62/−41, −62/−40	−80/−20, −60/−40	−65/−45, −90/−40
Fuc4NAc-ManANAc	−42/−17, −72/−40	−36/−17, 30/−20	10/−25, 0/−40

[a] The first pair of values refers to the first disaccharide moiety of the heptasaccharide model.
[b] The second pair of values refers to the second disaccharide moiety of the heptasaccharide model.

distances, particularly for ManANAc-H-1/GlcNAc-H-4, while only the internal residue presents good concordance for ManANAc-H-1/GlcNAc-H-6. With regard to GlcNAc-Fuc4NAc, two experimental NOEs were observed, GlcNAc-H-1/Fuc4NAc-H-4 and GlcNAc-H-1/Fuc4NAc-H-3. The average distances for the first linkage are of 2.61 and 2.67 Å, respectively, while the corresponding distances for the second GlcNAc-Fuc4NAc fragment are 2.42 and 2.60 Å. There is satisfactory agreement with the observed values, considering the experimental errors in the integral measurement and in the isolated spin pair approximation. Finally, the internal Fuc4NAc-ManANAc residue shows a Fuc4NAc-H-1/ManANAc-H-4 distance of 2.35 Å, and a Fuc4NAc-H-1/ManANAc-H-3 of 3.70 Å, while the same distances for the terminal reducing disaccharide unit are 2.61 and 2.98 Å, respectively. It can be observed in Table 2 that the experimental distances are closer to those observed for the internal moiety.

Non-restrained trajectory.—In order to evaluate the influence of the NOE restraints in the results of the MD simulation, an identical calculation was performed, but removing the restraints. The corresponding trajectory plots are given in Fig. 5. It is observed that there are important changes in the population distribution of the different areas with regard to the restrained simulation. Thus, although the trajectory stayed in low energy regions for most of the time, there is a significant amount of time in which conformers far from the global minimum are sampled. The average Φ/Ψ angles and interproton distances are also given in Tables 2 and 3. It is evident that there are notable changes in the conformational behavior, which can be evaluated with the help of the experimental data. In principle, it can be deduced that the restrained simulation provides a much better agreement with the observed results than the non-restrained simulation. In addition, the consideration of mobility around the whole low energy regions of the constituent disaccharides provides a satisfactory match between observed and expected results.

Lateral chains conformation.—The simulations showed very fast interconversion around the two possible rotamers for the acid group in the mannuronic acid moiety, while oscillation around the three staggered rotamers of the Fuc4NAc methyl group was also observed. With regard to the GlcNAc hydroxymethyl group, for the internal residue, the simulation stayed in the *gg* orientation for the whole simulation, while a ca. 2:1:1 equilibrium among *gg:gt:tg* was observed for the terminal residue. A similar behavior is found in the non-restrained MD simulation. Since no experimental coupling constants

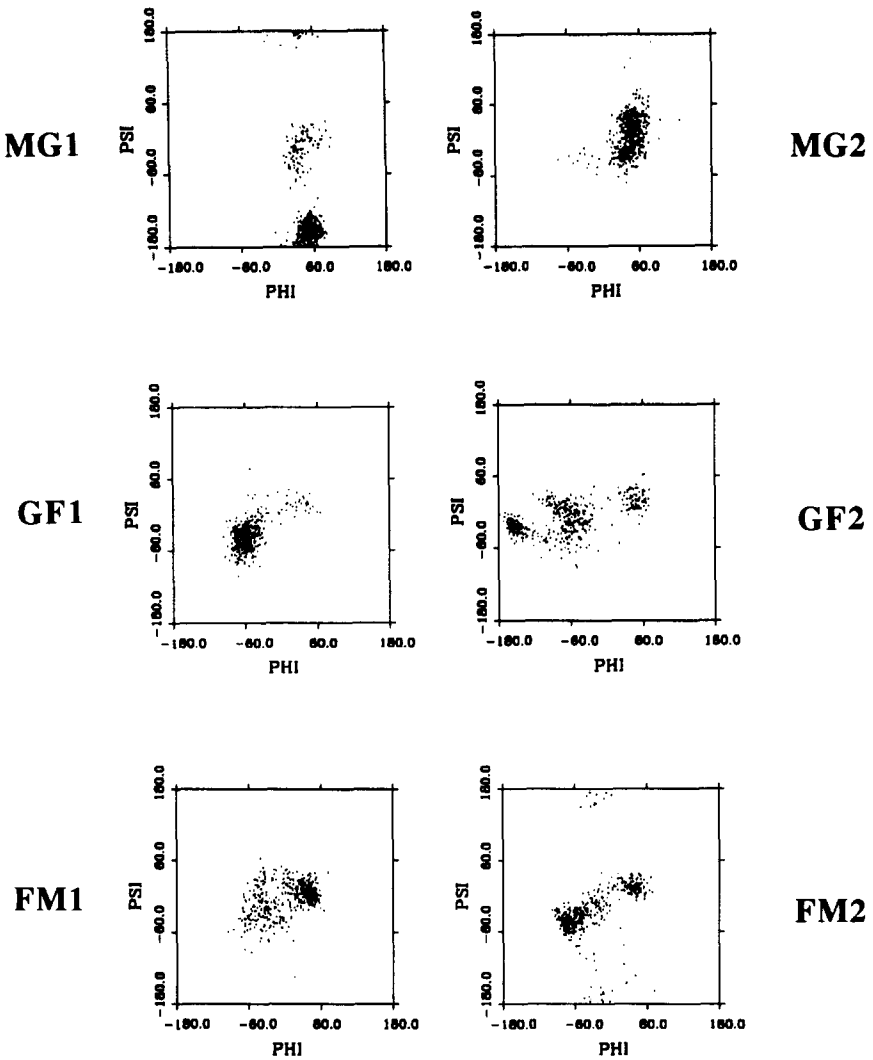

Fig. 5. Molecular dynamics Φ/Ψ trajectories corresponding to the unrestrained simulation.

could be measured, it is not possible to correlate these results with those existing in solution.

A view of the most favored conformer of the heptasaccharide model of the polysaccharide is depicted in Fig. 6. Nevertheless, given the extent of flexibility which is possible for every glycosidic linkage (ca. 10% of the complete potential energy surface), it is expected that the polysaccharide may adopt a variety of three-dimensional shapes. In fact, when the dodecasaccharide is built from ϕ/Ψ conformers belonging to the low energy regions for every glycosidic linkage, it can be observed that it may adopt a concave shape (Fig. 7, top). Slight variations of Φ/Ψ angles ($\pm 15°$) around the global

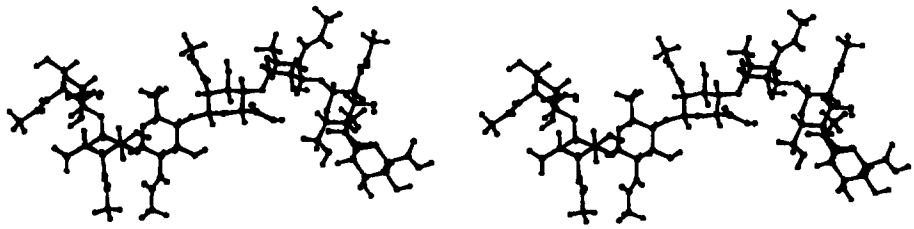

Fig. 6. Stereoscopic view of the most favored conformer of the heptasaccharide model of **1**, according to the restrained molecular dynamics.

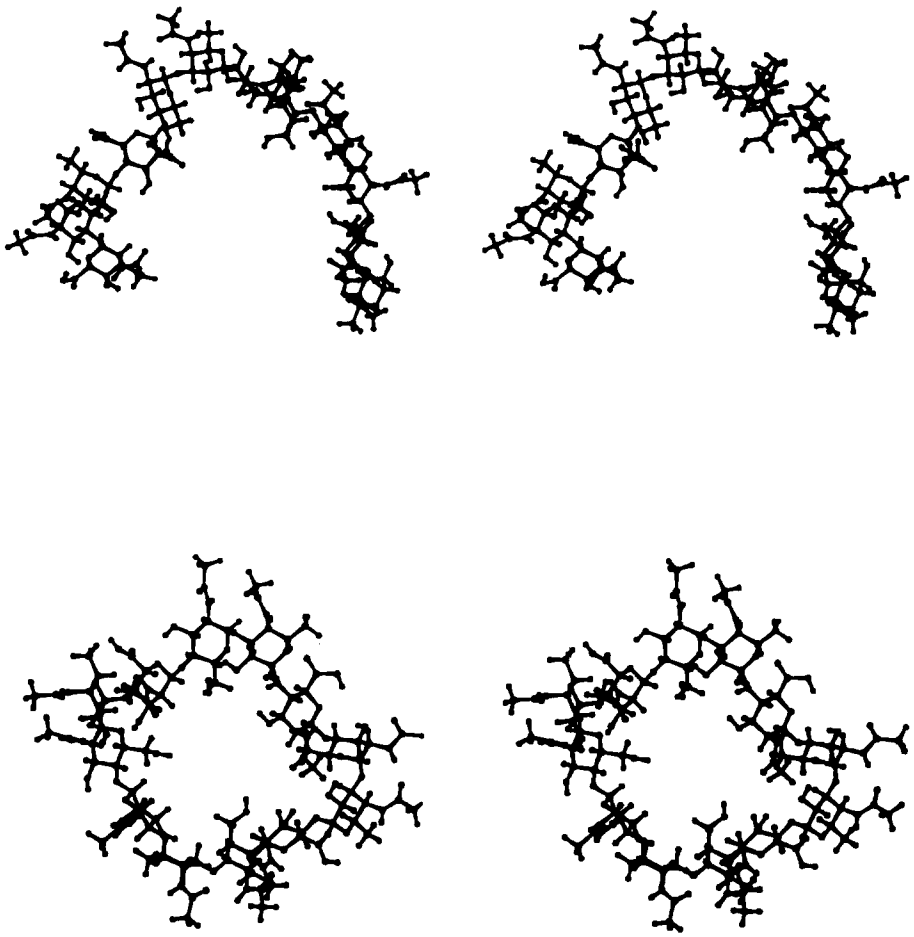

Fig. 7. Top: stereoscopic view of the dodecasaccharide model of **1**, built from Φ/Ψ conformers belonging to the low energy regions for every glycosidic linkage. Bottom: stereoscopic view of the dodecasaccharide model after slight variations of Φ/Ψ angles ($\pm 15°$) to get a cyclic structure.

minima for these linkages, bring into close proximity the anomeric reducing end oxygen and O-4 of the terminal ManANAc moiety (Fig. 7, bottom). Therefore it could be possible that in some species or under determined experimental conditions, a cyclic molecule could be formed as described for ECA from *Shigella sonnei* and *Yersinia pestis*.

3. Conclusions

According to NMR spectra, the polysaccharide isolated from *E. coli* shows a linear structure. Regarding the three-dimensional structure of ECA, two conclusions can be drawn: there is a significant amount of conformational freedom for the polysaccharide and, at least, for this system and with the conditions employed herein, the use of the theoretical simulations alone is not enough to accurately predict their conformational behavior. It seems necessary to run much longer MD simulations or to include explicit water molecules or both factors to satisfactorily predict conformational properties of this system. Unfortunately, both requirements imply the use of a much more than significant amount of computer time, which is, in most of the cases, far from being available. In addition, while the use of a force field of sufficient accuracy is absolutely necessary, there is still much debate about the validity and scope of the force fields currently used. Finally, it seems that the use of a few weak experimental restraints in the MD simulations, provides a satisfactory agreement between observed and expected conformational data, and, as stated by Homans and coworkers [9], is a useful approach to deriving the solution conformation of oligo- and polysaccharides.

The basic conformational features in terms of Φ/Ψ angles do not vary significantly from the linear to the cyclic form and agree with the observations of either linear or cyclic polisaccharides isolated from different sources.

4. Experimental

Sample.—The polysaccharide was found to co-purify with a chemotactic protein, Che Y [17], from *Escherichia coli* as well as with different mutants of this protein. The mutants were obtained by site direct mutagenesis using a method based from the polymerase chain reaction, as previously described [18]. Detailed procedures of the cloning, expresion and purification have been described elsewhere [19]. The sugar moiety was isolated from 1 mL of 0.33 mM protein solution in Tris (pH 8.0, 5 mM) by phenolisation (8 times) with equal volume of phenol/chloroform/isoamyl alcohol in relation 25/246/1 at pH 8.0. The aqueous phase was washed 3 times with pure chloroform to remove any excess of phenol. Then, it was diluted to 1 mL in water and dialysed overnight against water with a spectrapor 6 membrane (cut-off: 1000). The sample was concentrated to 0.5 mL by evaporation, and the purity was checked by electrospray mass spectrometry.

NMR experiments.—NMR spectra were recorded using 1 mM samples in 90%/10% H_2O/D_2O or D_2O at pH 7.0, on a Bruker AMX 600 (Homonuclear experiments) at

25°C and 35°C and on a Varian Unity 500 spectrometer (HSMQC) at 25°C. Proton chemical shifts were referenced to internal sodium 3-trimethylsilyl (2,2,3,3,-$^2H_4$) propionate. Carbon chemical shifts were referenced to external dioxane at δ 67.4 ppm.

The COSY [20], TOCSY [21], ROESY [22] and NOESY [23] experiments were performed in the phase sensitive mode using the time proportional phase incrementation [24]. Typically, a data matrix of 512 × 2K points was used to digitize a spectral width of 6000 Hz. 64–80 scans were used per increment with a relaxation delay of 1 s. Prior to Fourier transformation, zero filling was used in F_1 to expand the data to 1K × 2K. Various methods of resolution enhancement were used including shifted sine-bell or squared-sine-bell window functions, and base line correction was applied in both dimensions. The corresponding shift was optimized for every spectrum.

The TOCSY experiments were performed using MLEV-17 for mixing and 60 ms mixing time. The mixing time in the NOESY and ROESY spectra was set to 150 and 200 ms, respectively. In ROESY experiments the rf carrier was set at δ 6.0 ppm to minimize spurious Hartmann–Hahn effects [25].

The NOESY spectrum was integrated using standard Bruker software. The total intensity of the added F_1 cross-sections containing diagonal and cross-peaks was given a 100% value [26]. The NOESY intensities were employed for the estimation of interproton distances, using the so-called isolated spin-pair approximation (ISPA) [12].

The pure absorption one-bond proton–carbon correlation experiments were collected in the ^{1}H-detection mode at 500 MHz using the HSMQC [27] pulse sequences and a reverse probe. A data matrix of 256 × 2K points was used to resolve a spectral width of 10 000 Hz and 4500 Hz in F_1 and F_2, respectively. 16 scans were used per increment with a relaxation delay of 1 s and a delay corresponding to a J value of 152 Hz. A BIRD-pulse was use to minimize the proton signals bonded to ^{12}C. ^{13}C-decoupling was achieved by the WALTZ scheme. Squared cosine bell functions were applied in both dimensions and zero filling was used in F_1 to expand the data to 2K × 2K.

Molecular mechanics and dynamics calculations.—Glycosidic torsion angles are defined as Φ_H H-1′–C-1′–O-1′–C-X, and Ψ_H C-1′–O-1′–C-4–H-X. The previous step involved the generation of the corresponding rigid residue maps by using a grid step of 20°. Then, every Φ, Ψ point of this map was optimized using 200 steepest descent steps followed by 500 conjugate gradient iterations. Following this protocol, the maximum rms derivative in low energy regions was smaller than 0.05 kcal/mol/Å. Despite the restriction set around the glycosidic linkages (2500 kcal/mol/rad^2), deviations smaller than 0.3° in Φ/Ψ values were observed in high energy regions. The potential energy maps were calculated by using the AMBER [28] force field parametrised for carbohydrate molecules by Homans [14]. Only the *gg* conformation of the lateral chain was used for the glucose residue. The starting position for the secondary hydroxyl groups was set as *rr* (anti-clockwise). A dielectric constant of 78 D was used for the calculations. The combination of the global minima found for the constituent disaccharide entities of **1** was used to build the heptasaccharide structure, which was subsequently minimized. This geometry was then taken as starting structure for MD calculations in vacuo by using the AMBER force field as integrated in the Discover 2.9 program. The MD simulations were performed at 300 K with dielectric constants of 78 D, and a time step of 1 fs. The equilibration time was set to 150 ps while the total

simulation time was 500 ps. The temperature was controlled during the equilibration and simulation periods by coupling to a temperature bath, using an exponential decay constant of 0.1 ps [29]. During the equilibration, the velocities were rescaled when the difference between the actual and the required temperature was higher than 10°. Trajectory frames were saved every 1 ps. The trajectories were then examined with the Analysis module of INSIGHT II [30]. One simulation was performed with weak experimental restraints as deduced from NOESY experiments, while a second one was carried out under the same conditions, but removing these experimental constraints. These constraints were implemented for all the disaccharide fragments of the model as biharmonic restraints with lower and upper bounds of 2.0–2.7 and 2.3–3.1 Å, for strong and medium NOEs, respectively. No restraints were implemented for weak NOEs in order to avoid the possible generation of virtual conformations [10].

Acknowledgement

Financial support by DGICYT for projects Nos. PB93–0189 and PB93–0127 is gratefully acknowledged.

References

[1] H. Mayer and G. Schmidt, *Curr. Top. Microbiol. Immunobiol.*, 85 (1979) 99–153.
[2] S. Levasseur, M.O. Husson, R. Leitz, F. Merlin, F. Laurent, F. Peladan, J. Drocaut, H. Lecler, and M. van Hoegarden, *Appl. Env. Microbiol.*, 58 (1992) 1524–1529.
[3] C. Lugowski, E. Romanowska, L. Kenne, and B. Lindberg, *Carbohydr. Res.*, 118 (1983) 173–181.
[4] S. Basu, H-M. Kuhn, A. Neszmelyi, K. Himmelspach, and H. Mayer, *Eur. J. Biochem*, 162 (1987) 75–81.
[5] A. Dell, J. Oates, C. Lugowski, E. Romanowska, L. Kenne, and B. Lindberg, *Carbohydr. Res.*, 133 (1984) 95–104.
[6] E.V. Vinogradov, Y.A. Knirel, J.E. Thomas-Oates, A.S. Shashkov, and V.L. L'vov, *Carbohydr. Res.*, 258 (1994) 223–232.
[7] K.G. Rice, P. Wu, L. Brand, and Y.C. Lee, *Curr. Opin. Struct. Biol.*, 2 (1993) 669–674.
[8] A.D. French, V.H. Tran, and S. Perez, in A.D. French and J.W. Brady (Eds.), *Computer Modelling of Carbohydrate Molecules*, ACS Symposium Series 430, American Chemical Society, Washington, DC, 1990, pp 191–212.
[9] (a) S.W. Homans and M. Forster, *Glycobiology*, 2 (1992) 143–151; (b) T.J. Rutherford, J. Partridge, C.T. Weller, and S.W. Homans, *Biochemistry*, 32 (1993) 12715–12724.
[10] O. Jardetzki, *Biochim. Biophys. Acta*, 621 (1980) 227–232.
[11] (a) B. Hardy and A. Sarko, *J. Comput. Chem.*, 7 (1993) 831–847; (b) A.J. Duben, M. Hricovini, and I. Tvaroska, *Carbohydr. Res.*, 247 (1993) 71–81; (c) A. Imberty, K.D. Hardman, J.P. Carver, and S. Perez, *Glycobiology*, 1 (1991) 456–484.
[12] D. Neuhaus and M.P. Williamson, *The Nuclear Overhauser Effect in Structural and Conformational Analysis*, VCH Publishers, New York, 1989.
[13] B.R. Leeflang, J.F.G. Vliegenthart, L.M.J. Kroon-Batenburg, B.P. van Eijck, and J. Kroon, *Carbohydr. Res.*, 230 (1992) 41–61.
[14] S.W. Homans, *Biochemistry*, 29 (1990) 9110–9118.
[15] (a) M.K. Dowd, A.D. French, and P.J. Reilly, *Carbohydr. Res.*, 233 (1992) 15–36; (b) P.C. Kline, A.S. Serianni, S.G. Huang, M. Hayes, and R. Barker, *Can. J. Chem.*, 69 (1990) 2171–2182.

[16] *Discover 2.9 Program*, Biosym Technol. Inc., San Diego, CA.
[17] J.B. Stock, A.M. Stock, and J.M. Mottonen, *Nature*, 344 (1990) 395–400.
[18] V.V. Filimonov, J. Prieto, J.C. Martinez, M. Bruix, P.L. Mateo, and L. Serrano, *Biochemistry*, 32 (1993) 12906–12921.
[19] M. Bruix, J. Pascual, J. Santoro, J. Prieto, L. Serrano, and M. Rico, *Eur. J. Biochem.*, 215 (1993) 573–585.
[20] W.P. Aue, E. Bartholdi, and R.R. Ernst, *J. Chem. Phys.*, 64 (1976) 2229–2246.
[21] A. Bax and D.G. Davis, *J. Magn. Reson.*, 65 (1985) 355–360.
[22] A.A. Bothner-By, R.L. Stephens, and J.M. Lee, *J. Am. Chem. Soc.*, 106 (1984) 811–813.
[23] A. Kumar, R.R. Ernst, and W. Wüthrich, *Biochem. Biophys. Res. Comm.*, 95 (1980) 1–6.
[24] D. Marion and K. Wüthrich, *Biochem. Biophys. Res. Comm.*, 113, (1983) 967–974.
[25] A. Bax and D.G. Davis, *J. Magn. Reson.*, 63 (1985) 207–213.
[26] J. Breg. L.M.J. Kroon-Batenburg, G. Strecker, J. Montreuil, and J.F.G. Vliegenthart, *Eur. J. Biochem.*, 178 (1989) 727–739.
[27] E.R.P. Zuiderweg, *J. Magn. Reson.*, 67 (1990) 565–569.
[28] S.J. Weiner, P.A. Kollman, D.A. Case, U.C. Singh, and G. Ghio, *J. Am. Chem. Soc.*, 106 (1984) 765–784.
[29] H.J.C. Berendsen, J.P.M. Postma, W.F. van Gunsteren, A. Di Nola, and J.R. Haak, *J. Chem. Phys.*, 81 (1984) 3684–3690.
[30] Insight 2.1.0 Program, Biosym Technol. Inc., San Diego, CA.